JOURNAL OF AIRCRAFT
Vol. 46, No. 1, January–February 2009

Aerodynamic Investigations of an Advanced Over-the-Wing Nacelle Transport Aircraft Configuration

Geoffrey A. Hill* and Osama A. Kandil†
Old Dominion University, Norfolk, Virginia 23529
and
Andrew S. Hahn‡
NASA Langley Research Center, Hampton, Virginia 23681

DOI: 10.2514/1.39730

The transonic aerodynamics of an advanced, over-the-wing nacelle, subsonic transport configuration are assessed using both Euler and Navier–Stokes computational fluid dynamics and results are compared to a similar configuration with an under-the-wing nacelle installation and a similar wing–body configuration. The over-the-wing nacelle configuration is designed with a novel inboard wing channel section between the nacelle and the fuselage that produces favorable aerodynamic interference and reduces the overall drag. Qualitative observations and quantitative drag computations are performed for the three configurations at a cruise Mach number of 0.78. It was found that, at the cruise point, the inboard wing channel section of the over-the-wing nacelle configuration effectively produces a favorable pressure distribution but that the overall drag, compared to the under-the-wing nacelle configuration, is higher. This excess drag, however, was found to be largely localized in the nacelle interior. Euler and Navier–Stokes computational fluid dynamics solutions were obtained for additional Mach numbers to assess the transonic drag–rise characteristics. The computational fluid dynamics solutions showed that the over-the-wing nacelle configuration has higher drag at lower Mach numbers than the under-the-wing nacelle configuration but experiences a milder overall drag rise and has lower drag at higher Mach numbers.

I. Introduction

ENGINE nacelle integration is a complicated and challenging aspect of commercial transport aircraft design. Both the nacelle geometry and its placement have a significant influence on a wide range of aircraft characteristics.

Historically, commercial transport designers have found that mounting engine nacelles on pylons, either under the wings or on the aft fuselage, generally provides the best overall solution to what is always a complex mix of design considerations. Another nacelle installation that has been used but historically has not been as successful is that of mounting the engines over the wing. Notable examples of aircraft with this installation include the Fokker VFW 614 [1], the Boeing YC-14 [2], the NASA/Boeing Quiet Short-Haul Research Aircraft [3], the Russian Beriev Be-200, the Japanese Aska, and the Honda Business Jet [4]. Despite their usage, the over-the-wing nacelle (OWN) integrations for these aircraft were generally motivated by special requirements such as short takeoff and landing, austere runway operations, water operations, or a larger passenger cabin. One major reason that OWN installations have generally been unpopular, particularly for passenger transports, is the unfavorable aerodynamic interference they create at medium speed and transonic cruise conditions. OWN installations generally disturb the wing's upper surface pressure distribution which leads to excessive interference, badly misplaced shocks, and large flow separations. The overall effect is increased drag and degraded cruise performance.

Kinney et al. [5] outline design advantages for commercial transports with OWN installations. First, the installation is more accommodating for high-bypass turbofans, which have large fan diameters and can present ground clearance problems when mounted under the wing. Because a bypass ratio is beneficial to both engine efficiency and low noise, and the trend of increasing it is likely to continue, OWN installations may prove increasingly necessary for future commercial aircraft. Another advantage of OWN installations is the potential for community noise reduction as the wing can be used to shield the engine exhaust noise from ground observers. By contrast, under-the-wing nacelle (UWN) installations actually lead to slightly amplified community noise levels because aft-radiated acoustic waves from the engine exhaust reflect downward off the wing's lower surface. With the unswept inboard section of constant thickness, there is also more room for wing fuel, allowing for an extended range. Other potential design advantages to using an OWN installation include the avoidance of foreign object damage, the elimination of thrust gates for flaps, lighter and less constrained landing gear installations, and increased crashworthiness for a collapsed-gear landing or a water ditching [5]. Further, these advantages come without the tradeoffs in center-of-gravity placement and tail size associated with aft-fuselage nacelle installations.

OWN transport configurations have been known for high drag and poor cruise performance for the reasons that were mentioned earlier. This reputation has been openly noted by some researchers [4–6] and also has been substantiated by a large volume of wind-tunnel work and analytical study. Some work, however, indicates otherwise. Kinney et al. [5] note a number of wind-tunnel experiments on OWN configurations that revealed some favorable interference effects. An additional experiment, conducted in the NASA Langley Research Center's 16-ft wind tunnel, that produced encouraging results was reported by Reubush [7]. This experiment examined several different nacelle positions on a standard wing and, in many cases, measured lower drag levels for the OWN configuration than a wing body alone at transonic Mach numbers. The computational fluid dynamics (CFD) and wind-tunnel development work for the Honda Business

Presented as Paper 670 at the 45th AIAA Aerospace Sciences Meeting and Exhibit, Reno, Nevada, 8–11 January 2007; received 13 July 2008; accepted for publication 21 September 2008.

*Former Graduate Student, Department of Aerospace Engineering; currently Aeronautical Engineer, 1011 Lockheed Way, Palmdale, California 93599. Senior Member AIAA.

†Professor and Eminent Scholar, Department of Aerospace Engineering, 1300 Elkhorn Avenue. Associate Fellow AIAA.

‡Aerospace Engineer, Aeronautics Systems Analysis Branch, Mail Stop 348. Member AIAA.

Jet also demonstrated that, with careful design, an OWN installation can produce favorable aerodynamic interference and acceptable cruise performance [4].

Another encouraging finding from previous OWN research is the high sensitivity of the upper surface wing flow and the corresponding drag on OWN configurations to local wing and nacelle contouring. Analytical shaping using streamline tracing techniques in [8], Euler CFD in [4], and Navier–Stokes CFD in [9] resulted in significant flow quality and drag improvements to the OWN configurations studied, although the installation penalties were not always entirely eliminated. Aside from these studies, however, this sensitivity has generally not be fully exploited in much of the OWN wind-tunnel research because of hardware fabrication costs.

II. Advanced Over-the-Wing Nacelle Transport Concept

A. Concept Description

Figure 1 shows an advanced concept for a commercial transport in the 150-passenger class with an OWN engine installation. This concept was originally conceived and designed by Kinney et al. and the description of the design and aerodynamics work is published in [5]. The concept was designed to specifically address the medium-speed interference and transonic aerodynamic problems and reduce the common drag penalties associated with OWN configurations. This first effort, although it did not solve the interference problems, did provide enough insight to further refine the configuration.

The novel feature of the wing planform design is the unswept inboard section with the extended chord. The unswept leading edge, counterintuitive for transonic wings, was employed after the potential flow CFD of the initial studies revealed that no drag benefit was obtained as a result of the sweep because of the close proximity of the nacelle to the fuselage. The chord of the inboard section is extended such that the leading edge comes close to the front face of the nacelle. This extension creates a channel that is intended to aggressively accelerate the flow and create a significant low-pressure region which acts on a forward facing surface to counteract the drag. This acceleration at transonic speeds, however, produces a stronger shock that is located farther forward than the normal supercritical 60–70% chord location. For this design, however, placing the shock at about 25% chord is desirable as this allows the supervelocity effects to create the low-pressure levels over the forward part of the wing and also allows the flow to recompress through the shock while the boundary layer is still thin and relatively stable. The loss in sectional C_l that inevitably occurs as a result of the forward shock is compensated for by the longer chord length. Outboard of the nacelle, the wing is a standard swept design with supercritical airfoil sections. For this design, the forward "thrust" effects from the aggressive upper surface expansion, created by the presence of the nacelle, are intended to outweigh the effects of momentum loss and increased shock-induced separation, and create an overall drag decrease.

The nacelle is mounted directly to the wing with no pylon. While the inlet is circular, the nozzle is a "D" shape, and the jet exhaust flows directly over the aft-wing surface. Use of an OWN installation also enables an inverted gull-wing dihedral distribution. Although creating a structural weight penalty because of discontinuous wing spars, this distribution allows for shorter landing gear, reduces the elevation of the thrust line and resulting adverse propulsive trim effects, allows reduction of aft-body upsweep, and lessens the increase in cabin noise by giving the acoustic waves from the jet less of a direct path to the windows. Another potential benefit is that the outboard section of the wing, given even modest dihedral, can act as a barrier to shield engine exhaust noise radiated to the sideline and this dihedral need not be constrained by the landing gear length.

a) Isometric view

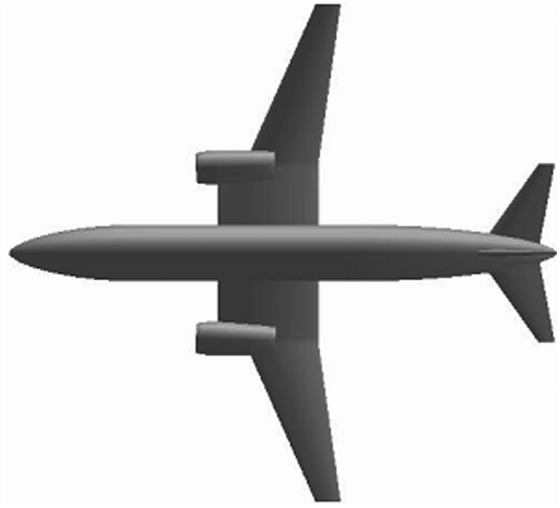

b) Planform view

Fig. 1 Early over-the-wing nacelle configuration.

B. Previous Aerodynamics Work

The transonic aerodynamics of the OWN concept shown in Fig. 1 were originally assessed in [5] by using a full potential CFD flow solver. Viscous effects were examined by using a coupled integral boundary layer method. For comparison, the aerodynamics of a conventional UWN configuration and a reference wing-body (WB) configuration with no nacelle were also assessed using the same methods. From the results of this original work, two significant findings emerged. The first was that the flow on the inboard wing section was clearly accelerated by the presence of the nacelle. Drag levels for the OWN configuration, although slightly higher than those for the UWN configuration at cruise conditions, were very close and the large drag penalties that are normally associated with OWN configurations were reduced. The second finding came from a transonic drag–rise analysis that was obtained through a Mach sweep. For Mach numbers well below the cruise point of 0.78, the OWN experienced inviscid drag levels as high as 12 counts more than the UWN configuration but experienced a much milder drag rise and had lower inviscid drag at the higher Mach numbers. Given these encouraging results, further unpublished work was conducted by Hahn and Kinney using Euler CFD. These additional results were consistent with those that were previously obtained with the full potential solver.

C. Present Aerodynamics Work

The work of this study was intended to further substantiate the previous transonic aerodynamic assessments of Kinney et al. [5] by using Navier–Stokes CFD. This assessment was considered necessary to fully address the effects of viscosity, an important physical ingredient of transonic flow. The presence of viscosity generally weakens shocks and changes their positions, often very markedly, as a result of the high sensitivity of local Mach numbers to

stream tube areas. Viscosity also leads to shock-induced flow separation, which can dramatically increase drag levels and change the overall drag–rise picture. Capturing this effect adequately requires a Navier–Stokes flow solver. The present assessment is also intended to provide more flow visualization to better study the qualitative aspects of the flowfield, particularly that of the inboard channel.

III. Analysis Tools, Grid Design, and Validation

A. Analysis Tools

The aircraft geometries for the CFD analysis were created using the NASA-developed parametric geometry tool Vehicle Sketch Pad (VSP), which allows a user to create simplified definitions of major aircraft components. The commercial CAD package Rhinoceros® was then used to further edit the VSP-generated surfaces and to create an Initial Graphics Exchange Specification (IGES) file for export to the CFD software. The TetrUSS CFD software suite [10] was used as the aerodynamic analysis tool set for this study. This software suite includes the programs GridTool, VGRID, USM3D, and various utilities. Geometry was prepared for grid generation using the GridTool program by defining nonuniform rational B-spline patches, background grid sources, and boundary conditions on the imported IGES files that were created by Rhinoceros. Grids were developed with the unstructured, tetrahedral grid generator VGRID, which constructs a viscous volume grid of thin, high-aspect-ratio, tetrahedral cells using an advancing layers technique and an inviscid volume grid of tetrahedral cells using an advancing front technique. The Euler and Navier–Stokes flow solver that was employed was USM3D, which uses an upwind, cell-centered, finite volume scheme with Roe's approximate Riemann solver. For the Navier–Stokes cases, turbulence was modeled through Reynolds averaging and the Spalart–Allmaras one-equation turbulence model. The solver was also run in fully turbulent mode with no transition.

B. Grid Design Considerations

Unstructured tetrahedral grids were used for the analysis and were constructed with established practices. The wing was significantly more resolved than the fuselage. No shock adaptation was applied, but the grid resolution was generally adequate to capture the shocks on the surface without excessive smearing. The leading edges of wings and nacelles were generally resolved to approximately 8 to 10 cells, and a spanwise cell stretching ratio of 6 to 1 was applied. A rectangular computational domain was used and was sized for transonic flow. The edges of the domain were located at 10 body lengths from the aircraft geometry in the longitudinal and vertical directions and 5 span lengths in the spanwise direction. The resolution in the outer domain was set to 12 cell lengths along the outer edge in the spanwise direction.

Viscous grids were constructed in VGRID from layers of thin tetrahedral cells created by slicing extruded prisms along the diagonal. The cell thicknesses in each layer were sized to adequately capture the boundary layer by using a stretching function in VGRID [11]. For Euler calculations, the trailing edges of wings, pylons, and nacelles were left closed and sharp. For Navier–Stokes calculations, the trailing edges were blunted, and a grid of one cell width was laid on the thin surfaces. The effects of the trailing-edge wake were then simulated with a transpiration boundary condition in USM3D.

C. DLR-F6 Validation

Because the present study involves the computation and comparison of drag levels between different configurations, a validation case was run to gain confidence in the grid design, modeling strategy, and code usage. The DLR-F6 wing–body–nacelle–pylon (WBNP) configuration was chosen as a validation subject because of its similarity to the configurations of interest, both in terms of geometry and flow conditions. Also, abundant transonic CFD and wind-tunnel results for the configuration were readily accessible through the AIAA 2nd Drag Prediction Workshop (DPW2) online data archive.[§] A Mach 0.75 cruise point drag polar and C_p distributions for several wing cuts of the WBNP configuration were run through USM3D and compared with the wind-tunnel data and the CFD results obtained by a few of the workshop participants.

Overall, the results of the USM3D runs, with the grid design and flow solver settings used in the present study, correlated sufficiently with the DPW2 CFD and wind-tunnel results despite some minor discrepancies. The drag levels at the cruise point were reasonably close to the wind-tunnel data at nominal C_L's, deviating by no more than 15 counts at a C_L of 0.5. The wing pressure distributions generally agreed with the wind-tunnel data, although the upper surface shock tended to be placed slightly forward of the location that was measured in the wind tunnel. This result, although systemic in many of the DPW2 CFD predictions [12], created some concern and led to an increase in grid resolution on the outboard wing. The agreement with the results that were obtained by the other workshop participants was generally adequate as well. More details on the validation and the full results are contained in [13]. Given the agreement, this validation case provided confidence that the results of the present study would sufficiently reflect the physics of the problem and enable an insightful comparison of the OWN configuration to the UWN and reference WB configurations. Also, because of the comparative nature of the present study, the absolute values of the drag predictions were of less concern than the incremental differences between the configurations.

IV. Problem Setup

A. Geometry

The aircraft geometries for the present study were created from the DLR-F6 WBNP geometry. The DLR-F6 was chosen as the base geometry, rather than the OWN and UWN test cases from previous studies, to minimally deviate from the validation case and also to test the robustness of the OWN inboard channel design concept with a slightly different gross configuration. Figure 2 shows the DLR-F6 WBNP configuration next to the UWN and OWN geometries to illustrate the evolution.

To create the UWN configuration, the DLR-F6 was scaled to the full-scale size of a general 150-passenger class transport by setting the wing span to 119.3 ft. The fuselage was smoothed, and both the windshield and horizontal tail mounting surface were eliminated. A wing/fuselage junction fairing was also added. The wing planform of the DLR-F6 was generally maintained, but the airfoils were changed to ones from the NASA SC(2)-04 supercritical family [14] because these were the airfoils used in the previous OWN studies. The wing thickness was set to 15% chord at the root, blended to 12% chord at the trailing-edge kink, and then maintained at 12% chord from the kink to the tip. The DLR-F6's nacelle was used but the pylon was substituted following the same design guidelines applied in the work of [5]. The pylon was also given a generous length, without any regard to nacelle ground clearance, to ensure that its effects on the installation drag would not be excessive and adversely affect the comparison. The reference WB configuration, which was intended for use in the comparison of relative nacelle installation penalties, was created simply by removing the nacelle and the pylon from the UWN configuration.

The OWN configuration was designed to be a minimal modification of the UWN configuration. The fuselage and the junction fairing were preserved, and only the wing and the nacelle were modified. The inboard section of the wing was unswept, and the leading edge was extended to nearly the front of the nacelle. The same SC(2)-04 airfoils were used for the wing of the OWN configuration. 15% chord thickness was applied to the whole inboard channel section, and 12% chord was applied to the outboard section. The dihedral distribution was modified to the inverted gull-wing configuration that was described earlier. Figure 3 shows comparisons of the UWN and OWN wing planforms and dihedral distributions.

[§]Data available online at http://aaac.larc.nasa.gov/tsab/cfdlarc/aiaa-dpw/Workshop2.

Fig. 2 Evolution of the UWN and OWN configurations from the DLR-F6 geometry.

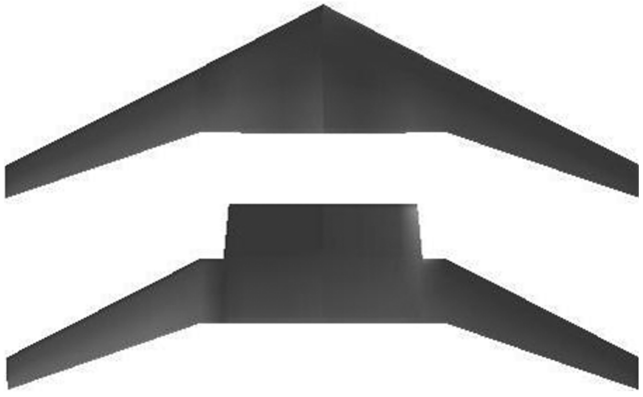

a) Wing planform comparison

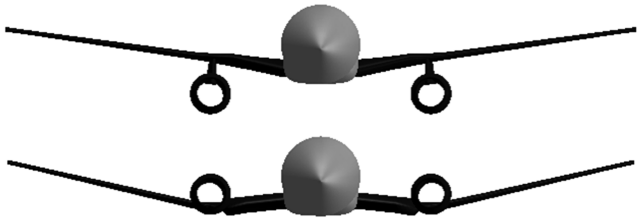

b) Wing dihedral comparison

Fig. 3 Comparison of the OWN and UWN geometries.

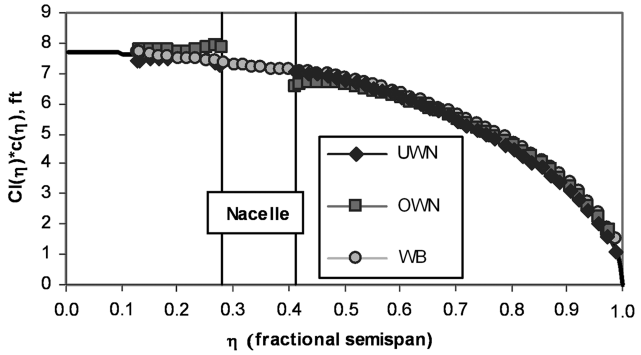

Fig. 4 Final span load distributions of the three configurations. Mach 0.78, C_L of 0.44.

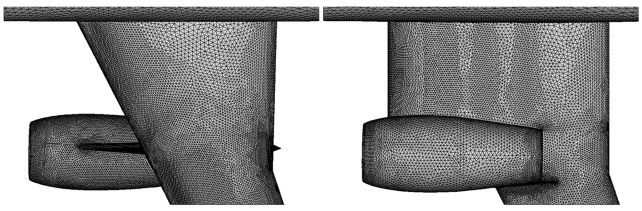

Fig. 5 Upper surface wing/nacelle regions for the UWN and OWN; standard NS grid.

The nacelle was elevated to a location where it provided an inboard channel wall of sufficient height, allowed a smooth transition from the nacelle interior to the aft-wing upper surface, and allowed the nacelle lower surface to be smoothly faired into the wing. The DLR-F6 nacelle geometry was maintained for the front half of the nacelle but was then transitioned to a D nozzle. Experimentation and modification were necessary on shaping the D nozzle to ensure that the exit area was of sufficient size to prevent choking inside the nacelle.

Finally, the wings of the OWN, the UWN, and the WB configurations were all twisted independently such that their aerodynamic span loads were closely matched. This was done to ensure that the drag comparisons would not be clouded by differences in lift-induced drag from span load inefficiencies. Figure 4 shows the span loadings for all three configurations along with an ideal ellipse. The twist distributions that were required for these span loadings were determined through an iterative process of modifying the geometry, regridding, and running Euler solutions at Mach 0.78 and C_L of 0.44. Figure 4 shows that, with the exception of the OWN configuration's inboard section next to the nacelle, the span loadings were relatively well matched to the ellipse.

B. Grids

The grids for all three configurations were designed using the previously discussed guidelines and the same basic parameters were applied to all three configurations. One of the Navier–Stokes grids (denoted as "standard NS grid") had a viscous portion that was sized with an initial y^+ value of 50, had 14 layers, and wall functions were used in the flow solver. A more expensive Navier–Stokes grid (denoted as "fine NS grid") was used for comparison and had a viscous portion sized with a y^+ value of 5, had 18 layers, and no wall functions were used in the flow solver. The inviscid portion of the fine NS grid was refined by decreasing the average linear cell dimension by 15%. The nacelles were treated as flow through with no propulsion effects or inlet-flow or exit-flow boundary conditions. This necessitated the gridding of the nacelle interiors and the creation of a smooth transition between the nacelle interior and the wing upper surface on the OWN configuration. Figure 5 illustrates the inboard wing/nacelle region of the UWN and OWN standard NS grids and Table 1 lists data for the three Euler grids and the six Navier–Stokes grids.

C. Computing Resources

The USM3D flow solver was run on Old Dominion University's Sun® Fire V20z dual-mode processor Linux cluster. Solutions were advanced by using implicit backward-Euler time integration with a Courant-Friedrichs-Lewy number of 150. The three criteria for solution convergence were an rms residual drop of at least 3 orders of magnitude, less than ± 0.0005 units variation in C_L, and less than ± 0.00005 units ($1/2$ count) variation in C_D. In every case, except for Navier–Stokes high-Mach cases, the C_D criteria was the last to be met. Euler solutions were generally run on 16 processors. Solutions from a cold start generally took 5 h of wall-clock time to converge. Warm starts from a converged solution with an angle of attack or Mach number perturbation generally took 3 h of wall-clock time. Navier–Stokes solutions were generally run on 32 processors for the standard NS grids and 64 processors for the fine NS grids. Solution wall-clock times on the standard NS grids were generally about 12 h from a cold start and 6 h from a warm start. Solution wall-clock times

Table 1 Grid information for all configurations

	UWN	OWN	WB
Euler grid			
No. cells surface grid	137,270	128,524	100,176
No. cells entire grid	8,638,585	7,687,469	8,721,269
Standard NS grid			
No. cells surface grid	153,540	142,878	119,080
No. cells viscous grid	3,883,818	3,541,536	2,711,019
No. cells entire grid	12,272,562	10,926,815	11,614,443
Fine NS grid			
No. cells surface grid	213,932	199,518	166,206
No. cells viscous grid	7,644,234	$\sim$7, 500, 000	5,379,210
No. cells entire grid	21,280,702	18,997,077	19,769,635
Viscous grid parameters	Standard NS grid	Fine NS grid	
y^+	50	5	
Thickness of 1st layer, in.	1.028E − 02	1.028E − 03	
No. of layers	14	18	

on the fine NS grids were generally about 20 h from a cold start and 10 h from a warm start.

V. Results and Discussion

A. Cruise Point Comparisons

It was first desired to compare the aerodynamics of the three configurations at a cruise point of Mach 0.78 and a C_L of 0.44. These values were the same as those used in the previous OWN studies and were considered to be closely representative of an actual 150-passenger transport. The Reynold's number was set to 41.1×10^6 based on a reference chord length of 22 ft (the chord length of the OWN configuration's inboard wing section) and the atmospheric conditions at an altitude of approximately 35,000 ft. The OWN configuration's half-wing planform area of 789 ft^2 was used as the reference area to normalize the force coefficients for all three configurations.

1. *Qualitative Observations*

Figures 6–10 illustrate the qualitative flow features of the OWN and UWN configurations by displaying the surface C_p contours and Mach number fields at several inboard and outboard wing cuts. The solutions were obtained from Navier–Stokes analysis on the fine NS grids. Several observations can be made. First, Figs. 6 and 10 reveal a significant and aggressive flow expansion region in the inboard wing channel section as expected. The shock line is positioned at roughly 35–40% chord, which is farther aft than the desired location of 25% chord. The shock line also meanders which indicates some flow separation. This separation is better observed in the Mach number cuts shown in Fig. 6. More flow expansion is seen on the wing section near the nacelle than on the wing section next to the fuselage, which also explains why the shock line gradually moves farther up the wing chord as the nacelle is approached. This extra expansion is likely the result of an overly acute angle at the wing/nacelle junction and the outboard tapering of the nacelle sidewall. Shock-induced flow separation is observed in the Mach number fields of Fig. 6, particularly next to the nacelle.

The outboard wing flow near the nacelle, shown in Fig. 7, appears to be influenced by the nacelle shock. This unfortunately limits the upper surface expansion to roughly 30–40% chord, which is much farther forward than the desired supercritical location of about 70% chord. The forward shock line in the outboard sections, however, is also observed on the UWN configuration, shown in Fig. 9, and appears to be an effect of the freestream Mach number and wing twist in this region. Closer to the nacelle, however, the shock off the nacelle appears to propagate outboard for a certain distance because the shock line of the wing curves slightly aft farther outboard. Despite this more forward shock location, the wing cuts shown in Fig. 7 do not reveal any significant boundary layer separation.

The UWN configuration's C_p contours in Fig. 8 show a gentler, more traditional supercritical upper surface flow expansion over nearly half the semispan. In the outboard sections, however, the shock line moves forward which limits the expansion just as it does on the OWN configuration. Another interesting flow feature (not shown) on the UWN configuration was observed on the inboard side of the pylon. Examination of surface C_p contours in that region indicated that a large expansion occurs, as a result of the flow constriction from the nacelle, pylon, and wing lower surface, which then creates a strong shock. This expansion and shock are, however, not excessive, because of the generous length of the pylon, and minimal flow separation was observed.

When all of the plots are compared, it is apparent that the inboard channel of the OWN configuration leads to a more aggressive upper surface expansion and a stronger shock than the UWN configuration which was expected. In addition, further examination of the shock strengths revealed that the selected cruise Mach number is more aggressive than it probably should be for the sweep and thickness of the wing. This fact likely contributes to a rather low lift-to-drag ratio,

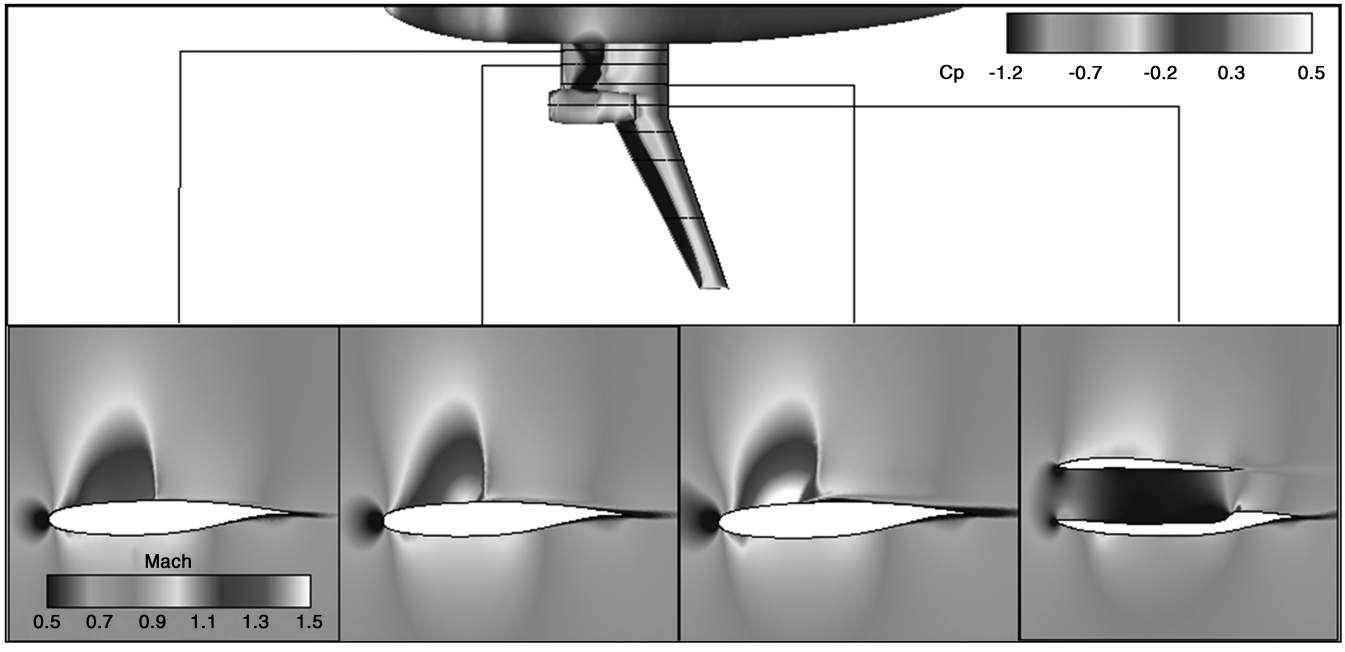

Fig. 6 OWN inboard wing cuts. Mach 0.78, C_L of 0.44, $Re_L = 41.1 \times 10^6$.

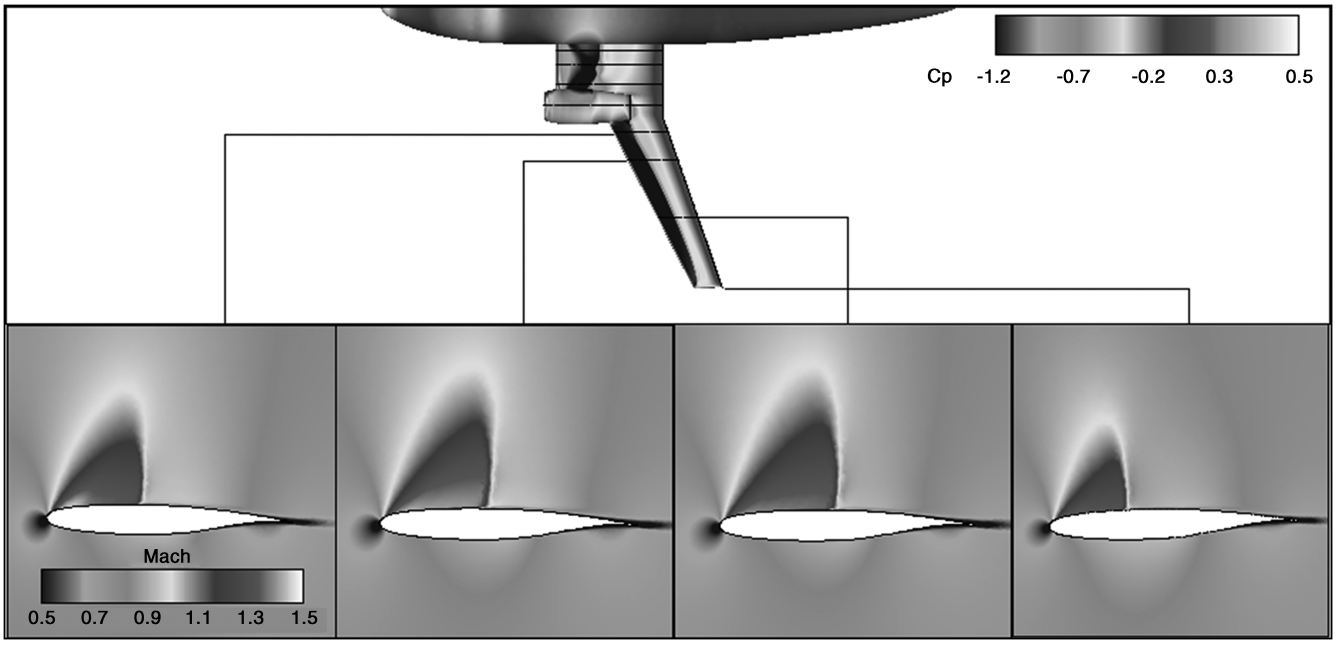

Fig. 7 OWN outboard wing cuts. Mach 0.78, C_L of 0.44, $Re_L = 41.1 \times 10^6$.

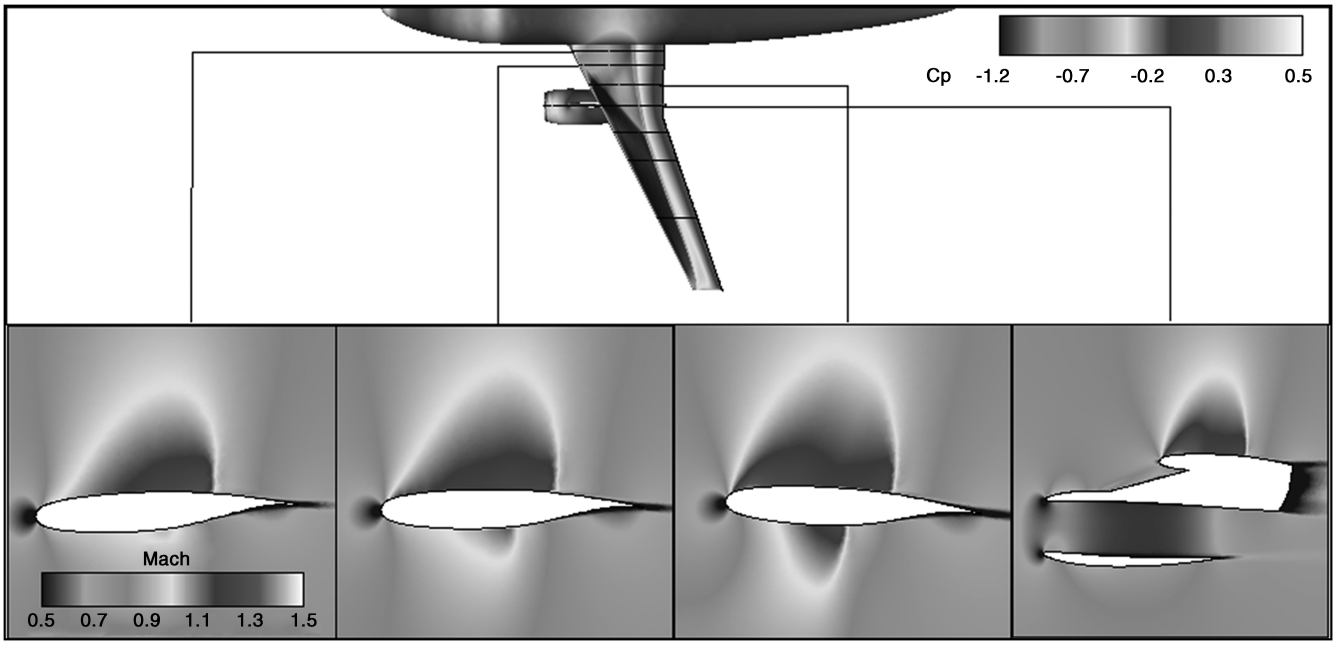

Fig. 8 UWN inboard wing cuts. Mach 0.78, C_L of 0.44, $Re_L = 41.1 \times 10^6$.

but the cruise point that was chosen still provides a suitable comparison.

2. Cruise Point Drag Levels

Table 2 shows the cruise point drag levels and the lift-to-drag ratios (L/D) for all three configurations. The drag coefficient is broken down into both pressure drag (C_{Dp}) and viscous drag (C_{Dv}), which are computed by USM3D from the pressure and shear stress integrations, respectively, over the aircraft surfaces. Wave drag and drag from flow separation are both captured in the pressure term and skin friction is captured in the viscous term. Comparing the fine NS grid total drag numbers, the OWN configuration has higher drag than the UWN configuration by 32 counts which results in 9.6% lower L/D. To put this drag difference between the OWN and the UWN configurations into a mission performance perspective, the Breguet range relationship is referred to the states whose range is directly

Table 2 Cruise point drag comparisons

Mach 0.78, C_L of 0.44, $Re_L = 41.1 \times 10^6$				
Euler grids	C_{Dp}	C_{Dv}	C_D	L/D
OWN			0.0188	
UWN			0.0178	
WB			0.0142	
Standard NS grids				
OWN	0.0265	0.0086	0.0351	12.5
UWN	0.0225	0.0091	0.0316	13.9
WB	0.0179	0.0076	0.0255	17.3
Fine NS grids				
OWN	0.0247	0.0087	0.0334	13.2
UWN	0.0210	0.0092	0.0302	14.6
WB	0.0169	0.0069	0.0238	18.5

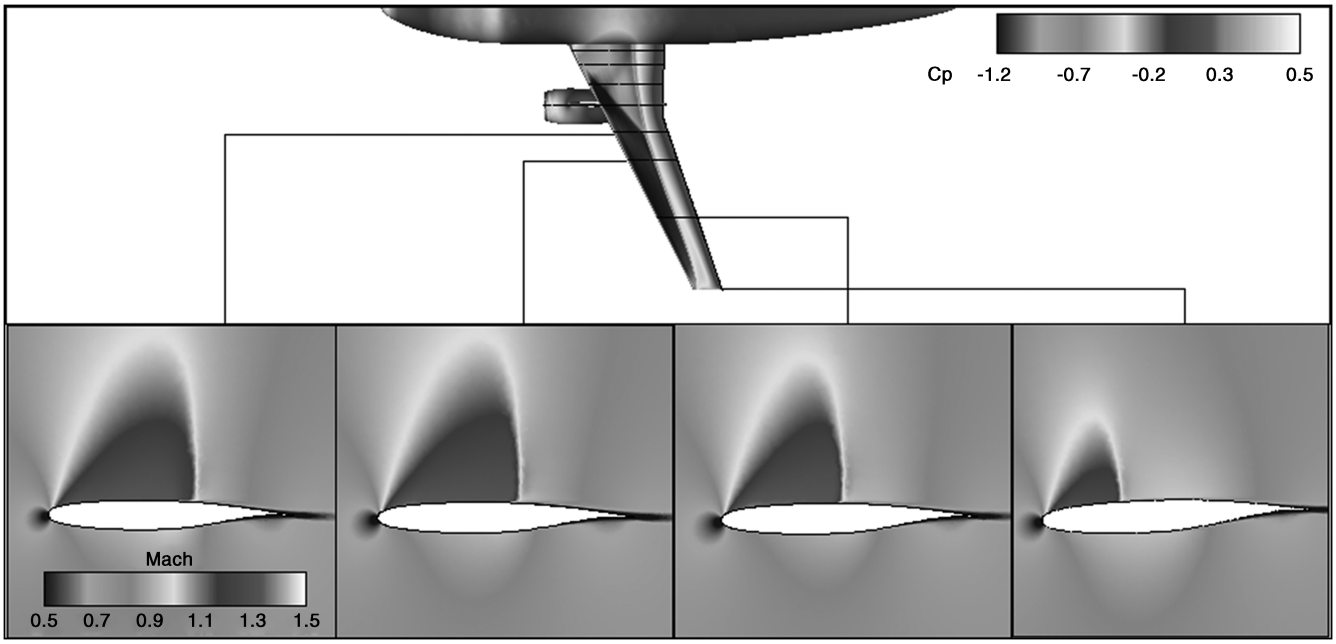

Fig. 9 UWN outboard wing cuts. Mach 0.78, C_L of 0.44, $Re_L = 41.1 \times 10^6$.

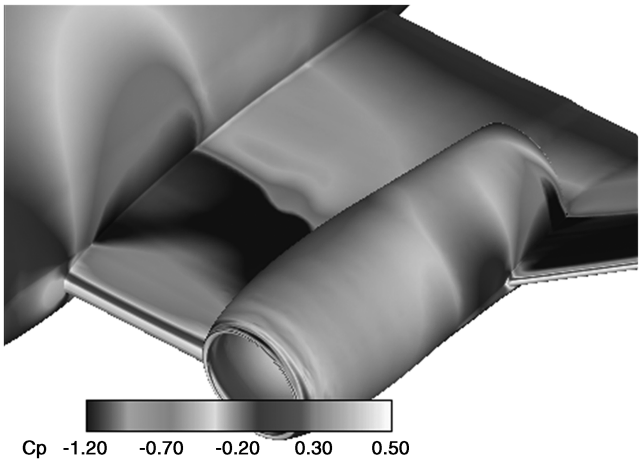

Fig. 10 Blow-up of OWN inboard wing channel. Mach 0.78, C_L of 0.44, $Re_L = 41.1 \times 10^6$.

proportional to L/D and proportional to the natural log of the reciprocal of the cruise mission segment weight fraction. Therefore, a reduction of 9.6% in L/D for the OWN configuration results in 9.6% less cruising range for an equivalent fuel burn. Alternatively, for an equivalent range, the reduced L/D means that the OWN configuration burns 1.0% more of its start-of-cruise weight in fuel (assuming a nominal jet transport cruise weight fraction of 0.9 for the UWN configuration). Although substantial, this excess in drag is relatively small compared with the large penalties observed in many wind-tunnel test cases of OWN configurations found in the literature. The drag excess is also small enough to preclude any immediate judgment that the OWN configuration is inherently less efficient than the UWN configuration, by virtue of its general design philosophy, or that the excess could not be removed with further design effort.

Examination of the fine NS grid drag components reveals that the OWN configuration actually has lower viscous drag levels by 5 counts, which is likely the result of a slight reduction in wetted area from the absence of a pylon. The drag excess for the OWN configuration therefore is the result of pressure drag from shocks and flow separation. A slight induced drag penalty may also be present because the span load distribution on the OWN configuration's inboard section was not entirely matched to the ellipse as shown in Fig. 4.

Comparison of the drag values between the standard and fine NS grids shows interesting results. The viscous drag levels that are computed on the two sets of grids are quite similar for the OWN and UWN configurations, which indicates that the wall functions and large y^+ value for the standard NS grids are adequate to model the boundary layer. The WB viscous drag levels, however, vary inexplicably by 7 counts (10.1% of total WB fine NS grid C_{Dv}). The pressure drag levels by contrast differ markedly between the two sets of grids. Table 2 shows that the standard NS grid solutions predict more drag than the fine NS grid solutions by 18 counts (5.4%) for the OWN configuration, 16 counts (5.3%) for the UWN configuration, and 10 counts (4.2%) for the WB configuration. The source of this pressure drag excess is most likely the larger trailing-edge wakes predicted on the standard NS grids that were observed on all configurations. Despite this discrepancy in absolute drag levels between the two sets of grids, however, the drag differences between the OWN, UWN, and WB configurations are nearly equal for both sets of grids. Also, aside from the larger wakes, the standard NS grids still capture all of the important flow features of the fine NS grids. In lieu of a more thorough grid refinement study with several resolutions, this standard/fine NS grid comparison provided enough confidence that the OWN, UWN, and WB configurations were being meaningfully compared for both resolutions and that the standard NS grids could be used in the Mach sweeps to save CPU time.

3. *Comparison of Spanwise Drag Levels*

To better isolate the source of the cruise drag excess for the OWN configuration and also quantify the effectiveness of the flow expansion produced by the inboard wing channel, the sectional pressure drag levels for several spanwise wing cuts were compared for all three configurations. The distribution of the sectional drag coefficient multiplied by the wing chord ($C_d{}^*c$) is plotted for all three configurations in Fig. 11. It is observed that the inboard channel feature of the OWN clearly produces a pressure drag reduction on the inboard wing sections as the $C_d{}^*c$ curve for the OWN configuration dips well below the other two curves. The wing sections that are next to the nacelle even experience a small amount of negative drag, which demonstrates that the suction effects from the aggressive flow expansion do indeed pay for the effects of the stronger shock.

Because the drag levels in the inboard wing section are lower on the OWN configuration, and those on the fuselage and outboard wing sections are largely comparable, it is apparent that the 37 counts (17.6% relative to total UWN fine NS grid C_{Dp}) of excess pressure

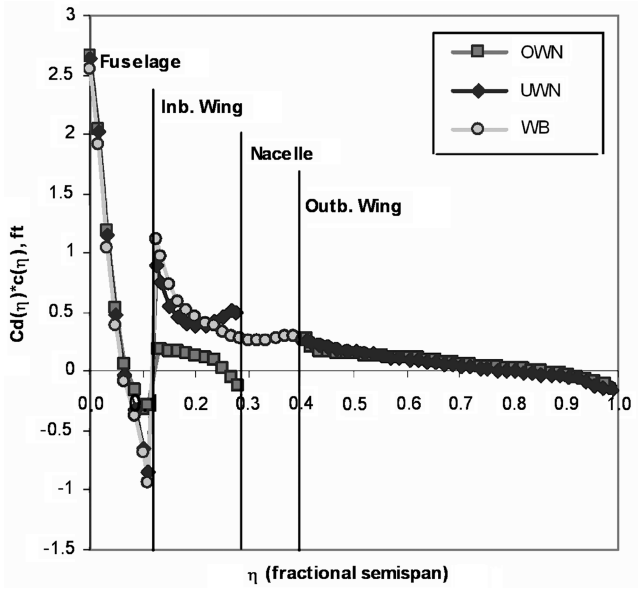

Fig. 11 Pressure $C_d{}^*c$ distributions for all three configurations.

drag on the OWN configuration primarily occurs in the nacelle region. Although the complete spanwise drag levels of the nacelle were not computed, because of the limitations of the data parsing program for more complicated geometry, the levels at two sections were evaluated to better isolate the drag excess. A comparison of the levels between the OWN and UWN configurations indicated that the drag excess was on the lower nacelle surface and quite possibly caused by the loft that transitions the OWN configuration's nacelle interior to the wing's aft upper surface. This transition surface, as shown in the nacelle cut of Fig. 6, presents some frontal area that is impinged by the flow. Because the nacelles in this study are flow through, this drag comparison would therefore substantially change with the addition of propulsion effects. The 32-count drag excess is therefore not a fundamental aspect of the configuration design of the OWN but merely appears to be caused by the flow-through nacelle aspect of the model.

The contributions of the pressure drag levels over just the inboard wing section to the total drag levels were computed for all three configurations by integrating the distributions in Fig. 11 over the fraction of the span that covers this section and normalizing by the reference area. This resulted in a total pressure drag of 11 drag counts for the OWN configuration (4.5% total OWN fine NS grid C_{Dp}), 54 counts for the UWN configuration (25.7% total UWN fine NS grid C_{Dp}), and 58 counts for the WB configuration (34.3% total WB fine NS grid C_{Dp}). The benefit of the low-pressure region on the OWN configuration is then 43 counts compared with the UWN configuration, and 47 counts compared with the WB configuration (a reduction of 17.4 and 19.0% relative to the total OWN fine NS grid C_{Dp}, respectively). It can therefore be concluded that the inboard channel feature of the OWN configuration does create beneficial interference effects and that the pressure drag savings from this feature are very significant. It should be emphasized, however, that the drag values computed are pressure drag only. Because the OWN configuration has more wetted area in the inboard section, these local drag benefits will be offset somewhat by the increased local skin friction.

B. Transonic Drag–Rise Comparisons

It was also desired in the present study to compare the transonic drag–rise characteristics of all three configurations using Navier–Stokes CFD analysis. Previous results in [5], which were obtained with a full potential solver, showed that the OWN configuration experienced a much milder drag rise than a comparable UWN configuration. Subsequent Euler analysis further substantiated these trends. It was therefore of interest to take the next step and examine the drag–rise characteristics while considering viscous effects and determine whether the same trends still existed.

Both Euler and Navier–Stokes solutions were computed on all three configurations for 11 Mach numbers in the transonic range from 0.6 to 0.85. The Navier–Stokes solutions were computed on the standard NS grids to save CPU time. At each Mach number, the C_L values of each configuration were converged to the target value of 0.44 by manually varying the angle of attack. A constant C_L drag–rise analysis was chosen over a constant lift analysis because the configurations that were being compared are fairly generic and because maintaining a constant C_L kept the lift-induced drag relatively constant through the range of Mach numbers which helped make the rise in wave drag and shock-induced separation drag more visible.

The Euler and Navier–Stokes transonic drag–rise results are shown in Figs. 12 and 13. The Euler results in Fig. 12 show the same trends as the previous studies of this OWN concept and therefore further substantiate those results. Because these results were obtained on DLR-F6-derived geometries, unlike previous studies, they also show that the general trends are not highly dependent on the gross configuration as much as on the engine installation. The OWN curve indicates higher drag levels at lower Mach numbers but then crosses the UWN curve at approximately Mach 0.79 and even crosses the reference WB curve at approximately Mach 0.82. These

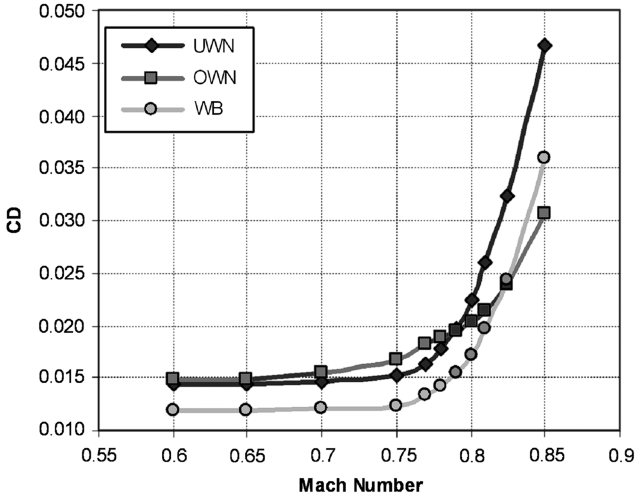

Fig. 12 Euler drag–rise trends.

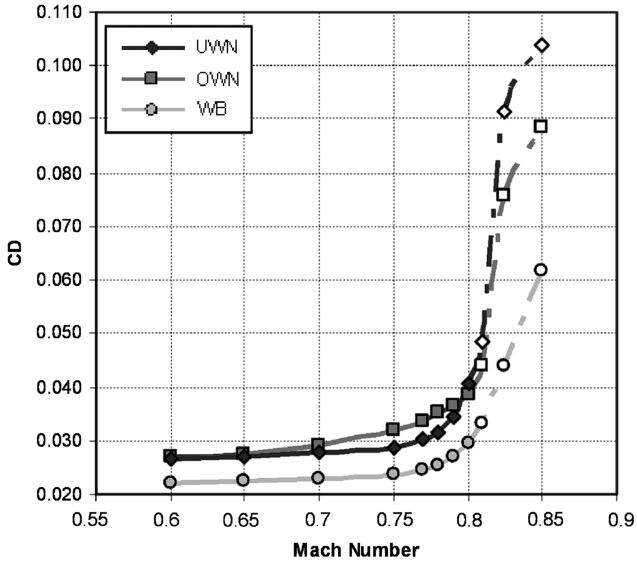

Fig. 13 Navier–Stokes drag–rise trends.

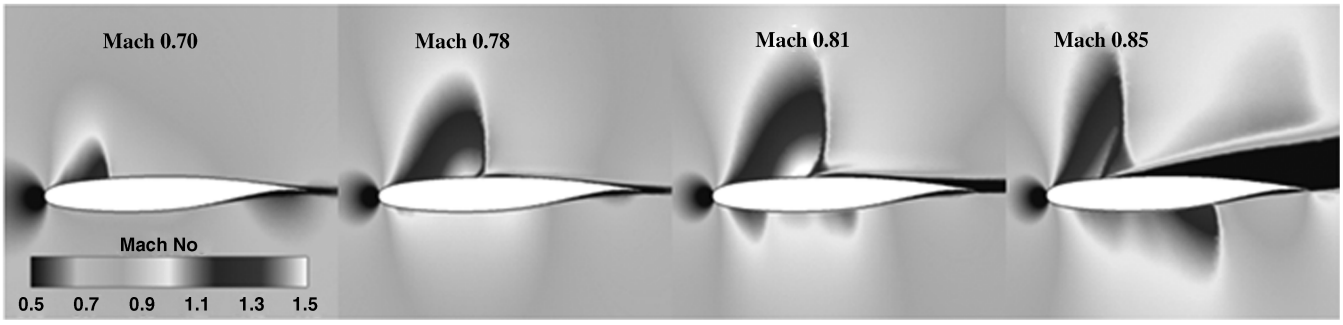

Fig. 14 Flowfields at the middle inboard wing section on the OWN configuration for different Mach numbers.

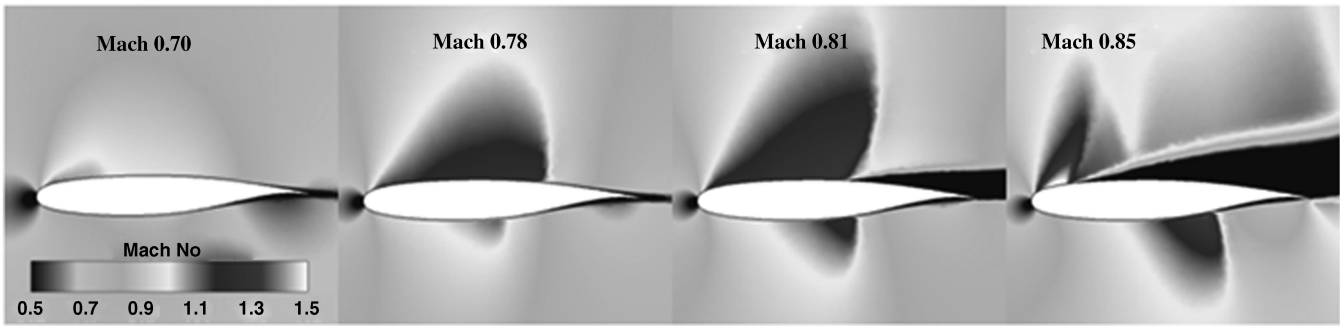

Fig. 15 Flowfields at the middle inboard wing section on the UWN configuration for different Mach numbers.

trends show that, in the absence of viscosity, the addition of the nacelle on the OWN configuration actually leads to a more aerodynamically efficient configuration that yields better cruise performance than a WB configuration alone at high transonic Mach numbers. In previous studies, this finding provided significant motivation for further research. At Mach 0.85, the OWN configuration experiences less drag than the WB configuration by 54 counts (15%), and less drag than the UWN configuration by 161 counts (34.5%). For inviscid flow, these reductions are very significant.

The Navier–Stokes drag–rise curves are shown in Fig. 13. The OWN configuration initially experiences drag levels that are very similar to those of the UWN configuration up to Mach 0.70. Then, the OWN configuration experiences more drag than the UWN configuration before the curves cross at about Mach 0.79, similar to the Euler trends. The trends in the higher Mach numbers above Mach 0.79, however, are different compared to the Euler trends. As a result of the effects of shock-induced flow separation, which begins to occur at about Mach 0.80 and becomes very significant at Mach 0.81 and above, the drag rise is much steeper.

Because of the presence of large-scale flow separation, the CFD solutions for all three configurations at Mach 0.81, 0.825, and 0.85 could generally not converge to the tolerances of ± 0.0005 units C_L and ± 0.5 counts C_D and required a substantial amount of flow solver run time for the C_L and C_D oscillations to be bounded. Bounds for C_L oscillations for these high-Mach cases ranged from ± 0.0005 to ± 0.005 and bounds for C_D oscillations ranged from ± 0.5 counts to ± 5 counts. Because of the difficult convergence, and because of the inherent difficulties of using Reynolds-averaged Navier–Stokes modeling to accurately compute drag with large-scale flow separation, the high-Mach cases are plotted with dashed curves and open points in Fig. 13 to denote a higher degree of uncertainty in this region compared to the lower Mach predictions. Despite this higher uncertainty, the trends still provide a useful assessment and the differences in drag are large enough to discern which configurations experience more drag rise than others. The OWN configuration still experiences much less transonic drag rise than the UWN configuration, which demonstrates that the nacelle installation likely outperforms the underwing pylon arrangement at the higher Mach numbers, even with the inclusion of viscosity. Unlike the Euler results, however, the OWN configuration experiences a significantly greater drag rise than the WB configuration, which indicates that the addition of the nacelle produces a drag penalty instead of a benefit in viscous flow.

Figures 14 and 15 illustrate the flowfields, for a few select Mach numbers, of the drag–rise analysis at cuts in the middle of the inboard wing sections of the OWN and the UWN configurations, respectively. At Mach 0.70, a small amount of supersonic upper surface expansion is observed on both configurations, but more is observed on the OWN configuration as a result of the channel flow acceleration. The flowfields for Mach 0.78 show larger amounts of supersonic upper surface expansion. For the OWN configuration, this expansion is concentrated on the front part of the wing and terminates in a strong shock at about 35–40% chord. The UWN configuration, however, displays a traditional supercritical flowfield with a gentler expansion and a weaker shock at about 70% chord. The flowfield at Mach 0.81 begins to reveal significant flow separation on both wings. Interestingly, less flow separation occurs on the OWN wing section even though the shock is clearly stronger. This effect is likely a result of the fact that the inboard sections of the UWN wing generally operate at slightly higher sectional C_l levels than the OWN sections do because the chords are shorter and the twist was adjusted to align the UWN span load with the OWN span load. The flowfields for Mach 0.85 show severe separation on both wings and even reexpansion and secondary shocks on the wake boundaries. The UWN configuration, in particular, is near full stall and actually experiences stall on a few of the other wing sections. This result demonstrates that, although the constant C_L drag–rise analysis was useful for the reasons mentioned earlier, the selected C_L of 0.44 is too excessive for the high-Mach numbers. It should also be cautioned again that the qualitative results at Mach 0.81 through 0.85, although insightful, are prone to more modeling uncertainty than the lower Mach predictions as a result of the large-scale flow separation.

VI. Recommendations for Further Study

Recommendations for further study are offered. First, the geometries that were studied were derived from the DLR-F6 WBNP configuration, and insufficient effort was expended in tailoring their outer mold lines for efficient aerodynamic performance. Although

use of the DLR-F6 as the base geometry kept the comparisons more in line with the validation results and established them in a firmer foundation of realism, the geometries did not represent well-performing airplanes. This was evident in the extensive flow separation that was observed at higher Mach numbers and the low lift-to-drag ratios. It would be of interest to consider another comparison case with a better performing subsonic transport as the base geometry.

Because the basic concept of the inboard wing channel design has been demonstrated to be effective, work should be performed in optimizing the wing and nacelle surfaces to adjust shocks, minimize flow separation, and create more efficient fairings between the wing and the nacelle. On the OWN configuration, the inboard channel flow should be optimized to produce maximum low-pressure "pull" with minimal shock-induced flow separation. The upper wing surface and nacelle sidewall represent degrees of freedom for such an optimization.

Fortunately, in recent years, advanced methods and increased computing power have enabled the discipline of CFD-based aerodynamic shape optimization to mature markedly. Both adjoint-based and knowledge-based methods (to name two examples), coupled with flexible and efficient geometry parameterization methods, have proven to be powerful tools for outer mold-line shaping. Given the high sensitivity of upper surface flow to nacelle and pylon contouring and the success of contouring efforts found in the literature, the application of these advanced tools and methods presents a promising avenue to address the over-the-wing nacelle problem.

Future comparisons should examine propulsion effects. Although only the external airflow is of interest, previous OWN work has found that higher speed jet flow from the engine exhaust can entrain surrounding air and create supervelocity effects that exacerbate the already existing shock strengths and flow separations. Some studies [15] have noted the importance of including propulsion effects, and several large-scale wind-tunnel tests have included turbofan engine simulators despite the increased cost and complexity. Although several CFD codes, including USM3D, have propulsion modeling capabilities, the inclusion of these effects was outside the scope of this study.

This study was limited to transonic aerodynamics and was therefore not comprehensive of all the design aspects of an over-the-wing nacelle transport aircraft. The advantages to the configuration were highlighted above, but additional design implications and tradeoffs with regards to weight, structure, trim, and noise were not examined. These trades, which in many regards constitute a significantly different overall design space, should be addressed but were outside the scope of this study. Ultimately, the consideration of an OWN configuration in any transport aircraft program will depend on a wide variety of factors that are both configuration and program dependent.

VII. Conclusions

A series of aerodynamic investigations was undertaken to examine both the inviscid and viscous flow characteristics of an advanced over-the-wing nacelle subsonic transport configuration using Euler and Navier–Stokes CFD. The results were compared with those from similar under-the-wing nacelle and reference wing-body configurations. These investigations included the qualitative study of the transonic aerodynamics and the computation of overall drag values at a design cruise point of Mach 0.78, an approximate altitude of 35,000 ft, and a C_L of 0.44. The investigations also included quantitative comparisons of the distribution of the sectional pressure drag levels for all three configurations and comparisons of both Euler and Navier–Stokes transonic drag–rise curves. The flow analysis was conducted with the TetrUSS CFD software suite, and aspects of the grid design and code usage were validated using the DLR-F6 WBNP configuration and the results from AIAA's 2nd Drag Prediction Workshop.

The drag levels for the OWN, UWN, and WB configurations computed at the cruise point showed that the OWN configuration had higher drag than the UWN configuration by 32 counts, a 9.6% difference in L/D. The increased low-pressure pull, caused by the aggressive flow acceleration in the OWN configuration's inboard channel, was quantified and the OWN configuration was found to have reduced pressure drag in this region that was as much as 43 counts less than that of the UWN configuration and 47 counts less than that of the WB configuration. This benefit demonstrated that the inboard channel design concept performs its intended function. It was also shown that the excess drag of the OWN configuration is all pressure related and is isolated in the nacelle's interior. This penalty would therefore change with the addition of propulsion effects.

The results of the Euler Mach sweep demonstrated that the OWN configuration experiences a much milder drag rise than the other two configurations and has lower drag than both the UWN configuration and even the reference WB configuration at the higher Mach numbers. In the Navier–Stokes Mach sweep, it was observed that the effect of the shock-induced flow separation made all the drag rises much more severe. The OWN configuration still experienced lower drag levels at the higher Mach numbers than the UWN configuration but higher drag levels than the WB configuration. Severe shock-induced flow separation at Mach numbers 0.81 and above was observed on all configurations.

Finally, this study presented an alternative to the traditional state-of-the-art transport nacelle installation and demonstrated that such a configuration need not be excluded from design trade studies because of a history of poor aerodynamic performance in previous research activities. Careful design of the integrated wing and nacelle structure, using modern CFD-based methods, can in general be employed to make an OWN a viable installation. The OWN configuration used in this study, particularly the inboard channel concept, was shown to be an effective design strategy for reducing the transonic drag normally experienced with the installation.

Acknowledgments

This research was supported by the Old Dominion University Department of Aerospace Engineering and by the NASA Langley Research Center. Special thanks go to Russell Thomas and Charlotte Whitfield for their support, and to Osama Kandil, Oktay Baysal, and Brett Newman for serving on the lead author's thesis committee.

References

[1] Kathen, H., "VFW 614, Quiet Short Haul Airliner," AIAA Paper 74-937, Aug. 1974.

[2] Grotz, C. A., "Development of the YC-14 Propulsion System," AIAA Paper 75-1314, Sept.–Oct. 1975.

[3] Cochrane, J. A., Riddle, D. W., and Stevens, V. C., "Quiet Short-Haul Research Aircraft—The First Three Years of Flight Research," AIAA Paper 81-2625, Dec. 1981.

[4] Fujino, M., and Kawamura, Y., "Wave-Drag Characteristics of an Over-the-Wing Nacelle Business-Jet Configuration," *Journal of Aircraft*, Vol. 40, No. 6, Nov.–Dec. 2003, pp. 1177–1184. doi:10.2514/2.7207

[5] Kinney, D. J., Hahn, A. S., and Gelhausen, P. A., "Comparison of Low and High Nacelle Subsonic Transport Configurations," AIAA Paper 97-2318, 1997.

[6] Ryle, D. M., Jr., Braden, J. A., and Gibson, J. S., "Upper Surface Blowing Aerodynamic and Acoustic Characteristics," AIAA Paper 77-608, June 1977.

[7] Reubush, D. E., "The Effect of Over-the-Wing Nacelles on Wing-Body Aerodynamics," AIAA Paper 78-1083, July 1978.

[8] Henderson, W. P., and Patterson, J. C., Jr., "Propulsion Installation Characteristics for Turbofan Transports," AIAA Paper 83-0087, Jan. 1983.

[9] Brodersen, O., Taupin, K., Maury, E., Spieweg, R., Lieser, J., Laban, M., Godard, J. L., Vitagliano, P. L., and Bigot, P., "Aerodynamic Investigations in the European Project ROSAS (Research on Silent Aircraft ConceptS)," AIAA Paper 2005-4891, June 2005.

[10] Frink, N. T., Pirzadeh, S. Z., Parikh, P. C., Pandya, M. J., and Bhat, M. K., "The NASA Tetrahedral Unstructured Software System," *The Aeronautical Journal*, Vol. 104, No. 1040, Oct. 2000, pp. 491–499.

[11] Pirzadeh, S. Z., and Frink, N. T., "Assessment of the Unstructured Grid Software TetrUSS for Drag Prediction of the DLR-F4 Configuration," AIAA Paper 2002-0839, Jan. 2002.

[12] Lee-Rausch, E. M., Frink, N. T., Mavriplis, D. J., Rausch, R. D., and Milholen, W. E., "Transonic Drag Prediction on a DLR-F6 Transport Configuration Using Unstructured Grid Solvers," AIAA Paper 2004-0554, Jan. 2004.

[13] Hill, G. A., "Aerodynamic and Acoustic Investigations of an Advanced Over-the-Wing-Nacelle Subsonic Transport Configuration," M.S. Thesis, Department of Aerospace Engineering, Old Dominion University, Norfolk, VA, 2007.

[14] Harris, C. D., "NASA Supercritical Airfoils: A Matrix of Family-Related Airfoils," NASA TP-2969, March 1990.

[15] Meleason, E. T., and Wells, O. D., "Investigation of Upper-Surface-Blowing Nacelle Integration at Cruise Speeds Utilizing Powered Engine Simulators," AIAA Paper 76-623, July 1976.